PROCEEDINGS, 49th Workshop on Geothermal Reservoir Engineering
Stanford University, Stanford, California, February 12-14, 2024
SGP-TR-227

The Role of Thermo-poroelastic Effects on Drilling Induced Fractures in the Utah FORGE Well 16A(78)-32

Ahmad Ghassemi[1], Zhi Ye[1,2], and Mudi Ratnayake[1]

1. Reservoir Geomechanics and Seismicity Research Group, The University of Oklahoma, Norman, OK 73069

2. Now at Department of Geology and Geological Engineering, South Dakota Mines, Rapid City, SD 57701

ahmad.ghassemi@ou.edu

Keywords: FORGE, Thermal Stress, Axial and Transverse Fractures, Stimulation

ABSTRACT

Borehole image logs of the Utah FORGE Well 16A(78)-32 reveal several zones of closely spaced fractures transverse to the wellbore. In places they occur alongside the usual axial drilling-induced tensile fractures. In this study, a 3D fully coupled thermo-poroelastic model is used to investigate the origin of these fractures. The model uses the thermo-poroelastic fictitious stress boundary element method. The fundamental mechanisms associated with cooling/heating of the rock in the context of drilling in enhanced geothermal systems are first described, and then the role of temperature and pore pressure in inducing failure and fractures in the well 16A(78)-32 (also referred to as 16A) is considered to ascertain the thermal nature of the observed fractures.

1. INTRODUCTION

Coupled thermal and poromechanical processes play an important role in many problems of interest in reservoir development such as drilling, stability of boreholes, and permeability enhancement in geothermal reservoirs. When rocks are subjected to temperature changes, the bulk solid and the pore fluid experience a volume change. A volumetric expansion can result in significant pressurization of the pore fluid depending on the degree of containment and the thermal and hydraulic properties of the fluid as well as the solid rock. Water in the pores may undergo pressure increases on the order of 1.5 MPa per Kelvin during heating for conditions typical of earth's upper crust (Williams and McBirney 1979). Consequently, a coupling of thermal and poromechanical, and chemical processes develops in geothermal reservoirs. These processes occur on various time scales and the significance of their interaction and coupling is dependent upon the problem of interest. For example, in drilling operations there is a strong coupling between thermal and poromechanical effects that has significant impact on the stress/pore pressure distribution around the wellbore and thus hole failure and fracture initiation. On the other hand, in hydraulic fracturing, the evolution of the fluid-rock mechanics coupling evolves rapidly (on the scale of minutes, hours to possibly days) compared to thermal processes, thus the thermal stress has little effect on the process in short time fracture propagation (aside from viscosity and density variations that can impact fracture growth). However, during a long injection phase (time scale of months and years), the thermo-mechanical coupling can no longer be neglected. Accordingly, different levels of coupling are necessary when studying wellbore failure, fracture propagation, and fluid circulation.

A thermo-poroelastic approach combines the theory of heat conduction with poroelastic constitutive equations (Biot, 1941), coupling the temperature field with the stresses and pore pressure. The governing equations of thermo-poroelasticity are (McTigue, 1986; Palciauskas and Domenico, 1982) are:

Constitutive equation (tension positive):

$$\sigma_{ij} = 2G\varepsilon_{ij} + \frac{2G\nu}{1-2\nu}\delta_{ij}\varepsilon_{kk} - \alpha\delta_{ij}p - \frac{2G(1+\nu)}{3(1-2\nu)}\beta_m\ \delta_{ij}T$$
$$\zeta = \frac{\alpha(1-2\nu)}{2G(1+\nu)}\sigma_{kk} + \frac{\alpha^2(1-2\nu)^2(1+\nu_u)}{2G(1+\nu)(\nu_u-\nu)}p + (\beta_p - \varphi\ \beta_f)T \quad (1)$$

Which are combined with the following to yield field equations to be solved for temperature, pore pressure, and stresses.

Equilibrium equation:

$$\sigma_{ij,j} = -F_i \quad (2)$$

Darcy's and Fourier's laws:

$$q_i = -\kappa \; p_{,i}$$
$$h_i = -k_m^T \; T_{,i} \tag{3}$$

Continuity and energy balance equations:

$$\frac{\partial \zeta}{\partial t} + q_{i,i} = \gamma_f \tag{4}$$

$$\frac{\partial \left(\rho_m C_m T\right)}{\partial t} + h_{i,i} = \gamma_h \tag{5}$$

where σ_{ij} is total stress tensor components, ε_{ij} is an average strain tensor components, p is induced pore pressure, T is induced temperature, ζ is fluid content change per unit reference volume, G is shear modulus, ν is drained Poisson's ratio, ν_u is undrained Poisson's ratio, δ_{ij} is Kronecker delta, α is Biot's effective stress coefficient, β_m is the volumetric thermal expansion of porous matrix, β_p is the volumetric thermal expansion coefficient of pore space, β_f is the volumetric thermal expansion coefficient of pore fluid and φ is porosity. where q_i is fluid flux in "i" direction (unit fluid volume per unit area), $\kappa = k/\mu$ is mobility (k is intrinsic permeability having dimension of length squared, and μ is fluid dynamic viscosity), h_i is heat flux in "i" direction (unit heat per unit area), k_m^T is thermal conductivity of porous matrix and pressure (p) and temperature (T) with subscript ",i" means its derivative with respect to that coordinate component. From the presented constitutive equations, conservation laws, and transport laws and the geometric relationship for small deformations, the following field equations (a modified Navier equation and pressure and temperature diffusion equations) can be derived:

Modified Navier equation:

$$G u_{i,jj} + \frac{G}{1-2\nu} u_{j,ji} - \alpha p_{,i} - \frac{2G\beta_m\left(1+\nu\right)}{3\left(1-2\nu\right)} T_{,i} = -F_i \tag{6}$$

where u_i are displacement components.

Pressure diffusion equation:

$$\frac{\partial p}{\partial t} = M\left[\kappa p_{,jj} - \gamma_f - \alpha \frac{\partial \varepsilon_{kk}}{\partial t} + \frac{1}{3}\left(\alpha\beta_m + \beta_f \varphi - \beta_p\right)\frac{\partial T}{\partial t}\right]$$
$$M = \frac{2G\left(\nu_u - \nu\right)}{\alpha^2\left(1-2\nu\right)\left(1-2\nu_u\right)}, \quad \beta_p = \varphi\beta_m \tag{7}$$

where M is Biot's modulus.

Temperature diffusion equation:

$$\frac{\partial T}{\partial t} = c^T T_{,ii} + \frac{\gamma_h}{\rho_m C_m}$$
$$c^T = \frac{k_m^T}{\rho_m C_m} \tag{8}$$

where c^T is the thermal diffusivity coefficient for matrix.

The field equations can be solved for certain problems such as heating/cooling of a borehole under 2D plane strain or complete plane strain conditions (e.g., Li et al. 1998; Tao and Ghassemi, 2010). General 3D problems require numerical modeling such BEM (Safari and Ghassemi, 2012; Safari and Ghassemi, 2015) and FEM (Lee and Ghassemi, 2010). Below we utilize both approaches to illustrate the fundamental physics and to investigate the nature of drilling induced fractures (DIFs) in the Utah FORGE well 16A(78)-32.

2. PORE PRESSURE AND STRESS DISTRIBUTION AROUND A WELLBORE IN THERMO-POROELASTIC ROCK

Consider a borehole with a radius R = 0.135 m in a reservoir that is at a temperature of 200 ˚C. The rock in the new section being drilled is cooled while the rock at shallower section is heated by the warmer drilling fluid. Let's consider a heated section where the wellbore wall is suddenly (rapid drilling compared to thermal and fluid diffusion time scales) cooled by water and maintained at 150 ˚C. For clarity of presentation and investigation of the role of temperature, only induced stress and pore pressures are studied. Thus, pore pressure and stress loadings are not considered to isolate thermal effects. The rock parameters are shown in Table 1 and correspond to Westerly granite.

Table 1: Thermo-poroelastic parameters for Westerly granite.

Shear modulus G	15,000 MPa
Biot's coefficient α	0.44
Drained Poisson's ratio ν	0.25
Undrained Poisson's ratio ν_u	0.33
Permeability coefficient κ	4×10^{-19} m^2
Porosity ϕ	0.01
Thermal expansion coefficient of solid α_m	2.4×10^{-5} K^{-1}
Thermal expansion coefficient of fluid α_f	3.0×10^{-4} K^{-1}
Thermal diffusivity c^T	5.1×10^{-6} m^2/s
Skempton's coefficient B	0.81
Fluid viscosity μ	3×10^{-4} Pa.s
Fluid diffusivity c	7×10^{-5} m^2/s

Figures 1 illustrates the profiles of induced pore pressure and the induced tangential stress around the wellbore. The rock around the wellbore is gradually heated and the borehole temperature is suddenly increased. A pore pressure increase is generated near the borehole at early times. With increasing time, the pore pressure peak is reduced and moves away from the well where it gradually recovers the original state. The magnitude of this pore pressure would be much larger depending on the rock type such as mudstones and or some tuffs (Tao and Ghassemi, 2010). Figure 1(b) presents the thermally induced tangential stress. With heating, a significant tangential tensile stress is induced around the wellbore. This is caused by the tendency of the rock to expand near the borehole wall. Away from the borehole wall, the magnitude of the induced tensile stress decreases and changes its sign at some point inside the formation i.e., turns into a tensile stress. This is because the expansion of the material near the borehole tends to push on the outer rock, thus inducing a tensile stress. The thermally induced radial and axial stresses (not shown) also show a significant increase by heating. At later times, the radial stress zone moves inside the formation while the magnitude of the "peak" increases.

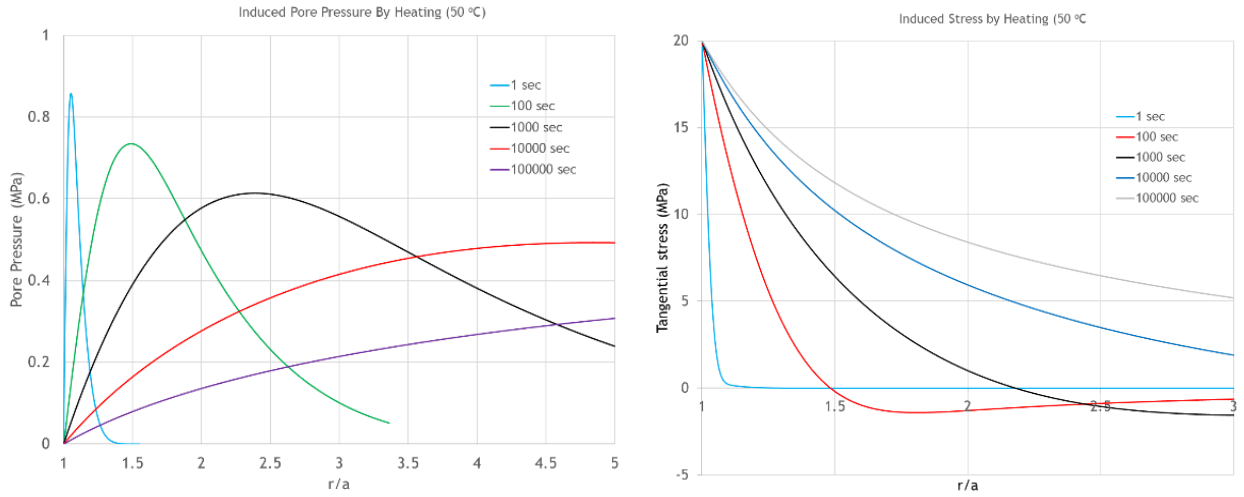

(a) **(b)**

Figure 1: The temporal evolution of the induced pore pressure (a) and the induced tangential stress (b) around the wellbore due to heating.

3. APPLICATION TO THE UTAH FORGE 16A

We now consider the contribution of thermal stresses to the drilling-induced fractures observed in Utah FORGE well 16A. In particular we are examining the section near the toe at the interval of 10,571 - 10,588 ft. (or 3,222 - 3227 m, measured depth), where some small axial fractures and many seemingly transverse fractures can be seen in the FMI (Figure 2).

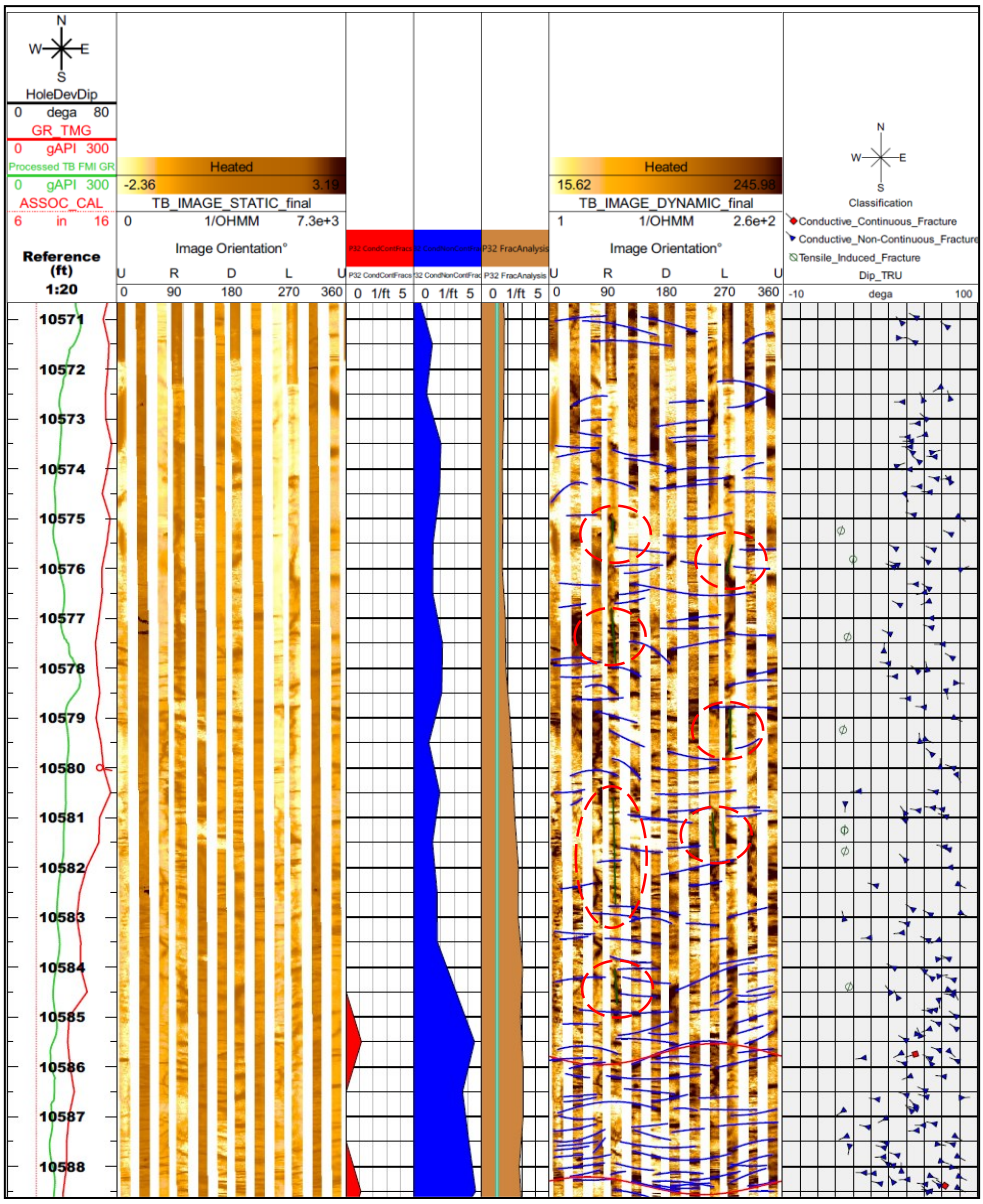

Figure 2: The FMI logs of FORGE well 16A(78)-32 at the interval of 10571-10588 ft. (or 3,222 - 3227 m, measured depth) reveal many short, closely-spaced transverse fractures (indicated by the blue, short transverse lines), along with some axial fractures (highlighted by red circles around the axial green lines).

Both axial and transverse fractures can be analyzed to ascertain lower bound for the S_{Hmax} magnitude (Ye at al., 2022, 2024). The occurrence of axial fractures requires that the effective tangential stress be tensile on some locations the wellbore wall along with sufficient magnitude to overcome the rock tensile strength. Using the properties shown in Table 2 we first simulate the wellbore stresses for a section at depth of ~10580 ft. (or 3225 m, measured depth) using an in-house wellbore stability model, based on 2-D plain strain analysis. The temperature and wellbore stress distributions are shown in Figure 3a and 3b. Figure 3b shows the distribution of effective stress components around the wellbore (along the maximum horizontal stress) after 2000 sec of cooling by 53 °C. As can be seen from the three stress components (induced plus in-situ), only S_{zz} is clearly tensile. The effective tangential stress is compressive so that the conditions for axial fracture are unlikely to be met. As shown in Figure 2, the fact that a few short lenticular fractures are observed is consistent with the stress analysis. These fractures could have been caused by heterogeneous thermal expansion, local pore pressure increases, and/or higher levels of cooling than assumed in the stress analysis. A 50% higher thermal expansion coefficient would lower the effective tangential stress to near tensile failure envelop.

Table 2: Input parameters for the modeling of the wellbore stress at 10580 ft. (or 3,225 m) in the Utah FORGE well 16A (see GDR for data from Utah FORGE projects OU-2-2404 and OU-5-2615, PI: A. Ghassemi).

Parameter	Value	Description
MD, ft. (m)	10,580 (3,225)	Measured depth
TVD, ft. (m)	8,385 (2,541)	Vertical depth
S_v, psi/ft (MPa/km)	1.13 (25.56)	Vertical stress
P_p, psi/ft (MPa/km)	0.44 (9.95)	Pore pressure
S_{hmin}, psi/ft (MPa/km)	0.73 (16.51)	Minimum principal stress
S_{Hmax}, psi/ft (MPa/km)	0.98 (20.29)	Maximum principal stress
α	0.76-0.81	Biot coefficient
B	0.54-0.57	Skempton's B coefficient
E, psi (GPa)	7910000 (54.54)	Young's modulus
v	0.29	Poisson's ratio
v_u	0.35	Undrained Poisson's ratio
c_f in^2/s (m^2/s)	0.0589 (3.8x10^{-5})	Hydraulic diffusivity coefficient
R, in (m)	4.375 (0.11)	Wellbore radius
ΔT, C°	53	Temperature difference due to cooling
T, psi (MPa)	1605 (11.07)	Tensile strength
C_o, psi (MPa)	13200 - 18300 (91.01 - 126.17)	Uniaxial compressive strength
k, in^2/s (m^2/s)	0.00218 (1.4x10^{-6})	Thermal diffusivity
α_T, 1/K°	0.000002	Thermal expansion coefficient

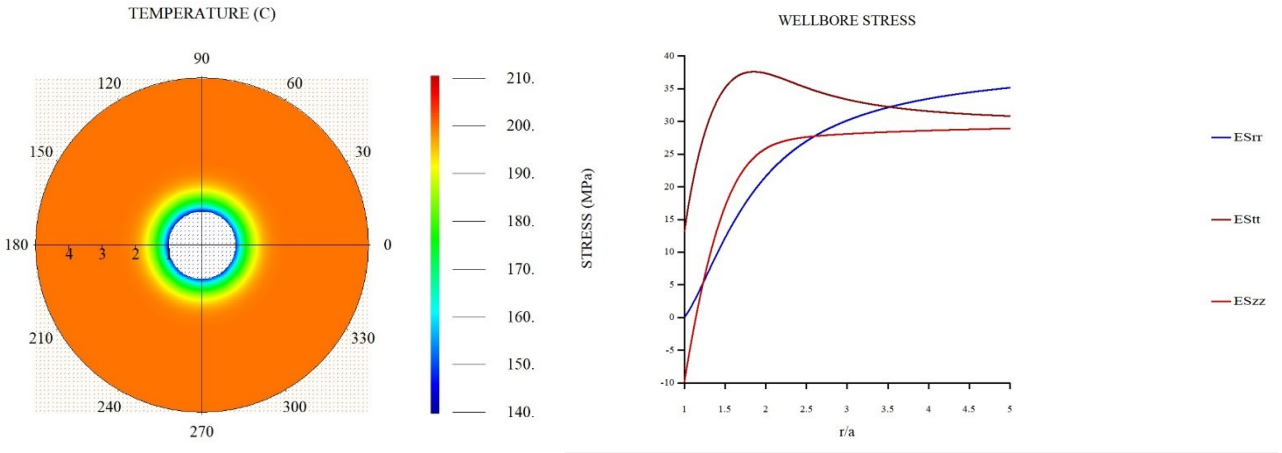

(a) **(b)**

Figure 3: (a) The temperature distribution around the wellbore; (b) the effective stresses around the wellbore. The blue curve indicates the effective radial stress (S_{rr}), the red curve represents the effect axial stress (S_{zz}), and the dark-red or brown curve indicates the effective tangential stress (S_{tt}).

The contour plots of the effective stress components around the wellbore are shown in Figure 4. The effective axial stress is tensile over a zone engulfing the wellbore and as one might expect a zone of tensile failure would develop as shown in Figure 2. As can be seen in Figure 4(c), the tensile failure stress zone is limited to a small region (blue).

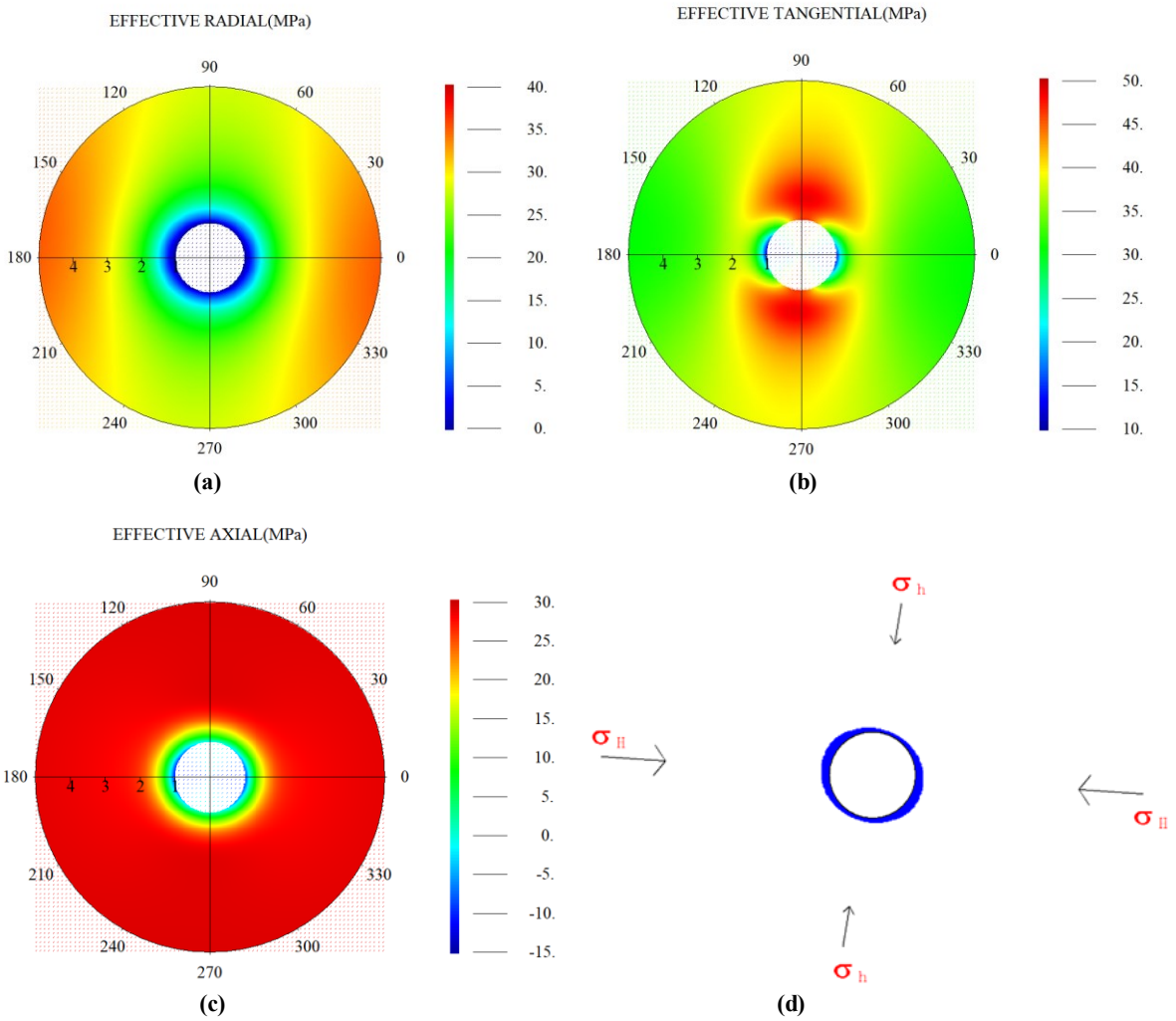

Figure 4: The contours of effective radial stress (a), effective tangential stress (b), and effective axial stress (c). The orientation of in-situ stress around the wellbore is shown in (d).

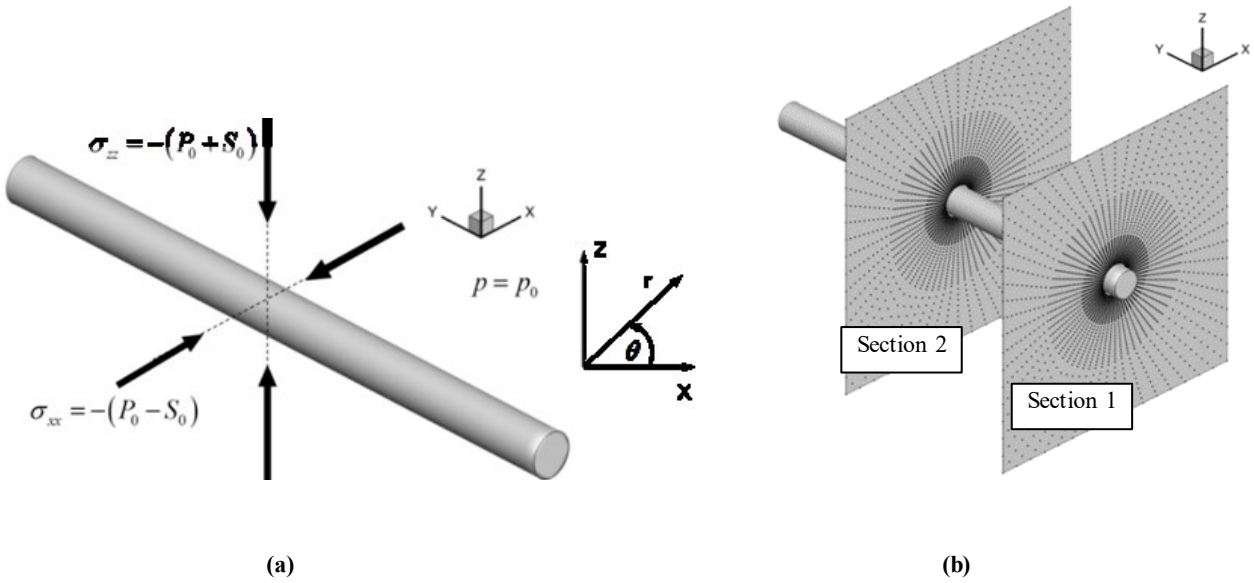

Figure 5: (a) The 3D sketch depicting the in-situ stress field around a wellbore; (b) the sections of the wellbore that were used for stress analysis.

As indicated before, the general problem of wellbore stability would require a numerical approach. We have an in-house 3D fictitious stress model (Safari and Ghassemi, 2012) that is used to treat the problem in 3D. For this purpose, we consider a section of the wellbore as shown in Figure 5. To eliminate end-effects, we consider the stresses in Section 2 in Figure 5(b) so as to make comparison with the 2D plane strain analysis meaningful.

The results shown in Figure 6 are in good agreement with the 2D solution (Figure 3 and Figure 4). The minor differences between 3D solution and 2D solution are attributed to the discretization and more importantly the 3D nature of the diffusion and deformation in the numerical model. Figure 6c illustrates the distribution of the minimum principal stress around the wellbore. The condition for transverse fracturing includes a tensile tangential stress or a tensile minimum principal stress all around the wellbore. In this case, the second condition is clearly satisfied so that the transverse fractures observed in the FMI log are likely caused by mud cooling. It should be noted that the mud cooling has a positive effect on shear failure tendency that is it reduces the likelihood of breakouts. As a result, breakout analysis for stress estimation should consider the thermo-poromechanical effects (Tao and Ghassemi, 2010; Tran et al., 2010).

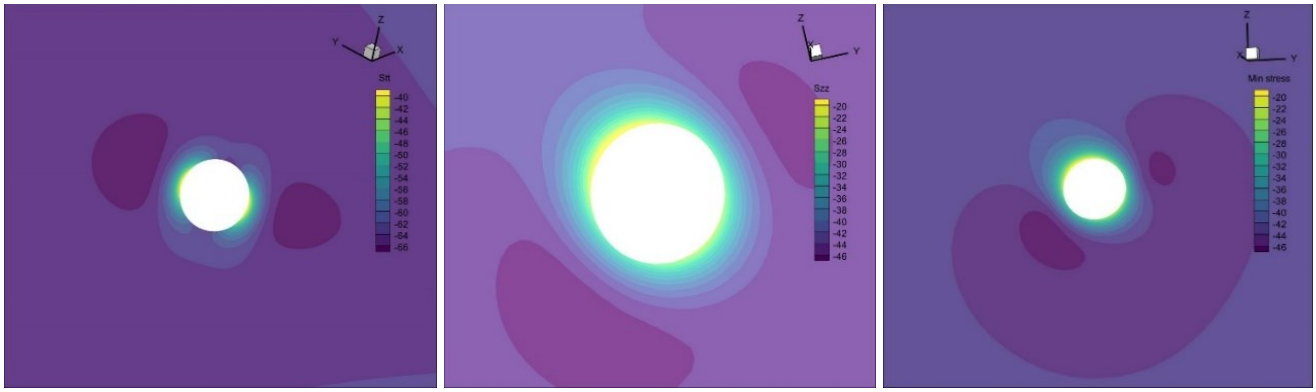

(a) **(b)** **(c)**

Figure 6: (a) Total tangential stress (S_{tt}); (b) total axial stress (S_{zz}); (c) total minimum principal stress around the wellbore. Considering a near wellbore pore pressure equal to the mud pressure of 25 MPa, the axial and the minimum principal stress become tensile.

4. CONCLUSIONS

This study employing fully coupled thermo-poroelastic models, has shed light on the mechanisms of drilling induced axial and transverse fractures observed on the image logs of Utah FORGE Well 16A(78)-32. The investigation reveals the significant role of thermal and poromechanical interactions in wellbore stability during geothermal drilling operations. Key findings indicate that some of the observed transverse fractures alongside axial drilling-induced fractures are predominantly influenced by thermal stresses from drilling activities. Furthermore, it appears that most of these transverse fractures remained stable, characterized by their short length and failure to span across the entire wellbore, as evidenced in image logs. This stability suggests that the combined effects of mud pressure and cooling were inadequate to propagate these fractures. The insights gained from this study enhances the understanding of fracture dynamics in geothermal reservoirs and underscores the importance of integrating thermal and mechanical factors in wellbore stability analysis for effective and sustainable geothermal energy extraction. Future efforts should focus on refining predictive models and expanding the scope of research to various geological settings for a comprehensive understanding of fracture mechanisms in enhanced geothermal systems.

ACKNOWLEDGEMENTS

This project was supported by the Utah FORGE project sponsored by the U.S. Department of Energy, through the project “Application of Advanced Techniques for Determination of Reservoir-Scale Stress State at Utah FORGE.”

REFERENCES

Biot, M. A. General theory of three-dimensional consolidation. Journal of applied physics, 12(2), (1941), 155-164.

Brudy, M. and Zoback, M. D., 1999. Drilling-induced tensile wall-fractures: implications for determination of in-situ stress orientation and magnitude. International Journal of Rock Mechanics and Mining Sciences. vol. 36, no. 2, pp. 191–215. X.

Ghassemi, A. and Zhang, Q. 2004. Poro-thermoelastic mechanisms in wellbore stability & reservoir stimulation. Proceedings, 29th Stanford Geothermal Workshop, Stanford, CA (2004).

Lee, S. H. and Ghassemi, A., 2010. A Three-Dimensional thermo-poro-mechanical finite Element analysis of a wellbore on damage evolution. Proc. 44th US Rock Mechanics Symp., Salt Lake City, UT.

Lee, Sang H. and Ghassemi, A. Themo-poroelastic analysis of injection-induced rock deformation and damage evolution. Proceedings, 35th Workshop on Geothermal Reservoir Engineering Stanford University, Stanford, CA (2010).

Li, X., Cui, L., and Roegiers, J.-C. 1998. Thermo-poroelastic Analyses of Inclined Boreholes. SPE.

McTigue, David F. Thermoelastic response of fluid-saturated porous rock. Journal of Geophysical Research: Solid Earth 91, no. B9 (1986): 9533-9542.

Palciauskas, V. V., and P. A. Domenico. Characterization of drained and undrained response of thermally loaded repository rocks. Water Resources Research 18, no. 2 (1982): 281-290.

Safari, M. R. and Ghassemi, A. 3D modeling of natural fracture stimulation using a poroelastic displacement discontinuity method with slip weakening. In ARMA US Rock Mechanics/Geomechanics Symposium, pp. ARMA-2012. ARMA, 2012.

Safari, M. R. and Ghassemi, A. 3D thermo-poroelastic analysis of fracture network deformation and induced micro-seismicity in enhanced geothermal systems. Geothermics 58 (2015): 1-14.

Safari, M. R., & Ghassemi, A., 2012. 3D Modeling of Natural Fracture Stimulation Using a Poroelastic Displacement Discontinuity Method with Slip Weakening. Proc. American Rock Mechanics Association Symp.

Stephens, G., and Voight, B. Hydraulic fracturing theory for conditions of thermal stress. In International Journal of Rock Mechanics and Mining Sciences & Geomechanics Abstracts, vol. 19, no. 6, pp. 279-284. Pergamon, 1982.

Tao, Q., and Ghassemi, A. 2010. Poro-thermoelastic borehole stress analysis for determination of the in-situ stress and rock strength. Geothermics, 39(3), 250-259.

Tran, D.T., Roegiers, J.-C., Thiercelin, M. 2010. Thermally-Induced Tensile Fractures In the Barnett Shale And Their Implications to Gas Shale Fracability. 44th U.S. Rock Mechanics Symposium and 5th U.S.-Canada Rock Mec., Symp., Salt Lake City, Utah, June 2010.

Williams, H., and A. R. McBirncy, Volcanology, 397 pp., Freeman, Cooper, and Co., San Francisco, Calif., 1979.

Ye, Z. and Ghassemi, A. The Updated Wellbore Stress Models for Utah FORGE. Proceedings, 49th Workshop on Geothermal Reservoir Engineering, Stanford University, Stanford, CA (2024).

Ye, Z., Fang, Y., Ghassemi, A., and McLennan, J. A Preliminary Wellbore In-Situ Stress Model for Utah FORGE. Proceedings, US Rock Mechanics/Geomechanics Symposium, Santa Fe, NW (2022).